mined the fraction of the excess work dissipated during each of the three types of rapid motion: cavitation, plastic yield, and bridge rupture. Starting from any wall separation, one can cycle the walls outward by a given amount and then back to the initial separation. The total work done to perform such a cycle is equal to the energy dissipated. The work used to stretch films between rapid rearrangements was recoverable in the low-velocity limit. In contrast, each rapid rearrangement led to an amount of dissipation that was nearly independent of the rupture velocity. About 1/3 of the excess work was dissipated in each of the three types of rapid motion. We confirmed this division by performing simulations with a prenucleated cylindrical cavity in the initial configuration and calculating the extra surface area after bridge rupture (Fig. 1D).

Processes usually become reversible as the velocity decreases. The reason that the dissipation remained constant in glassy films was that they were always far from equilibrium during rapid rearrangements (*3*). Instantaneous velocities reached large values that were set by the yield stress of the glass rather than by the mean rupture velocity. Similar instabilities may be the origin of static friction in solid-on-solid sliding (*15*). Motion through rapid rearrangements was also observed at higher temperatures, particularly cavitation and bridge rupture. However, in this case the dissipation was velocity-dependent, and viscous dissipation dominated at low velocities.

In our simulations, the adhesive energy G for glassy films was approximately twice the reversible work. Comparable ratios have been measured in experiments on tightly cross-linked rubber on glass (*16*) and on adsorbed monolayers of short molecules (*17*). The latter studies have also shown that adhesion hysteresis becomes negligible when the adhesive enters a fluid state (Fig. 2). Ratios between G and *W* are orders of magnitude larger for commercial adhesives. Although they have much larger chain lengths and film thicknesses, these adhesives exhibit the same types of rapid yield events that are seen in our simulations, namely cavity nucleation, plastic flow, and stringing or crazing (*1, 2, 13*). We found that all of these processes dissipated more energy with increased film thickness and chain length. For example, the size of bridges and the amount of work done to stretch them grew linearly with chain length for lengths between 8 and 32 monomers. Somewhat larger chains should become entangled (*8*) and allow the formation of the extremely long bridges observed in crazes. Entanglement would also enhance viscous losses. Energy dissipated during plastic flow increased with the thickness of the flowing region and with the local yield stress. The latter is related to the internal friction between molecules and should be larger for realistic molecules than for our smooth chains. It may also be increased by introducing liquid crystalline order or hydrogen bonds between molecules. Both are present in silk, which is well known for its superior mechanical properties (*18*).

### REFERENCES AND NOTES

1. D. Maugis, in *Adhesion and Friction*, M. Grunze and H. Kreuzer, Eds. (Springer-Verlag, Berlin, 1990).
2. R. P. Wool, *Polymer Interfaces: Structure and Strength* (Hanser, Munich, 1995).
3. K. Kendall, *Science* **263**, 1720 (1994).
4. A. N. Gent and J. Schultz, *J. Adhes.* **3**, 281 (1972); A. N. Gent and S.-M. Lai, *J. Polym. Sci. B* **32**, 1543 (1994).
5. S. A. Joyce, R. C. Thomas, J. E. Houston, T. A. Michalske, R. M. Crooks, *Phys. Rev. Lett.* **68**, 2790 (1992).
6. P. A. Thompson, G. S. Grest, M. O. Robbins, *ibid.*, p. 3448; P. A. Thompson, M. O. Robbins, G. S. Grest, *Isr. J. Chem.* **35**, 93 (1995).
7. M. P. Allen and D. J. Tildesley, *Computer Simulation of Liquids* (Clarendon, Oxford, 1987).
8. K. Kremer and G. S. Grest, *J. Chem. Phys.* **92**, 5057 (1990).
9. J. G. Kirkwood and F. P. Buff, *ibid.* **17**, 338 (1949); P. A. Thompson, W. B. Brinckerhoff, M. O. Robbins, *J. Adhes. Sci. Technol.* **7**, 535 (1993).
10. J. N. Israelachvili and A. Berman, *Isr. J. Chem.* **35**, 85 (1995).
11. S. Granick, *Science* **253**, 1374 (1991); G. Reiter, A. L. Demirel, S. Granick, *ibid.* **263**, 1741 (1994).
12. P. H. Mott, A. S. Argon, U. W. Suter, *Philos. Mag. A* **68**, 537 (1993).
13. H. H. Kausch, Ed. *Crazing in Polymers* (Springer-Verlag, Berlin, 1983).
14. U. Landman, W. D. Luedtke, N. A. Burnham, R. J. Colton, *Science* **248**, 454 (1990); R. M. Lynden-Bell, *ibid.* **263**, 1704 (1994).
15. G. A. Tomlinson, *Philos. Mag.* **7**, 905 (1929); J. N. Glosli and G. McClelland, *Phys. Rev. Lett.* **70**, 453 (1993).
16. K. Kendall, *J. Adhes.* **7**, 55 (1974).
17. H. Yoshizawa, Y.-L. Chen, J. N. Israelachvili, *J. Phys. Chem.* **97**, 4128 (1993); M. K. Chaudhury and M. J. Owen, *ibid.*, p. 5722.
18. D. Kaplan, W. W. Adams, B. Farmer, E. C. Viney, Eds. *Silk Polymers* (ACS Symposium Series 544, American Chemical Society, Washington, DC, 1994).
19. We thank P. A. Thompson, G. S. Grest, P. M. McGuiggan, and J. N. Israelachvili for useful discussions. Support from National Science Foundation grant DMR-9110004, Petroleum Research Fund grant 28790-AC5,9, and the Pittsburgh Supercomputing Center is gratefully acknowledged.

18 August 1995; accepted 15 November 1995

# The Structure and Stability of Atomic Liquids: From Clusters to Bulk

Jonathan P. K. Doye and David J. Wales

Insights into the structure of simple liquids are presented from analysis of the effect of the range of interatomic forces on the multidimensional potential energy surfaces of bulk material and clusters. An understanding at the microscopic level is provided of how the liquid phase is destabilized in systems with very short-range interparticle forces. For small clusters bound by long-range interatomic forces, the lowest energy minimum has an amorphous structure typical of the liquidlike state. This suggests an explanation for the transition from electronic to geometric magic numbers (structures of special stability) observed in the mass spectra of sodium clusters.

The phase diagrams of simple substances depend sensitively on the form of the interatomic or intermolecular forces (*1*). In particular, the range of temperature for which a liquid-vapor transition can occur as a function of pressure decreases with the range of attraction (*2*). For example, the interparticle forces of some colloids (*3*) and perhaps $C_{60}$ (*4*) have such a short range that no liquid phase is observed—instead, there is only a single fluid phase. In contrast, the critical temperature for sodium is about seven times as large as the triple-point temperature because of the long-range interatomic forces. Here, we provide an understanding of this phenomenon at the microscopic level and relate it to structural models of liquids and glasses. Because these models often make use of results from cluster studies (*5, 6*), we consider finite clusters as well as bulk material. By understanding how the behavior of clusters is similar to or different from that of bulk material, we can address questions concerning the evolution of the

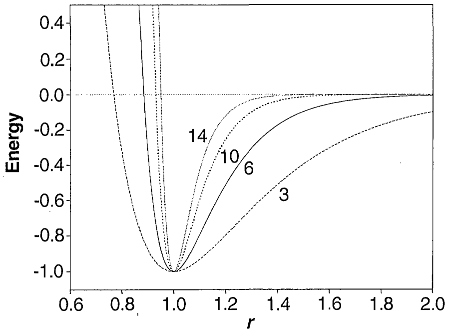

**Fig. 1.** The Morse potential for different values of the range parameter $\rho_0$ as marked. Quantities in all figures are in reduced units.

---

University Chemical Laboratories, Lensfield Road, Cambridge CB2 1EW, UK.

phase-like forms of clusters to the bulk limit and the transition from electronic to geometric magic numbers seen in the mass spectra of sodium clusters (*7, 8*).

We explored these issues by considering how the range of the interatomic forces affects the topology of the multidimensional potential energy surface of both bulk material and clusters. In particular, we focused on the local minima of the potential energy surface because these can reveal the "inherent structure" of the liquid, which is normally obscured by thermal motion (*9*). We used the Morse potential, which has a single adjustable parameter, $\rho_0$, that determines the range of the interparticle forces. In reduced units the potential energy may be written as

$$V_M = \sum_{i<j} e^{\rho_0(1-r_{ij})}[e^{\rho_0(1-r_{ij})} - 2] \qquad (1)$$

where $r_{ij}$ is the distance between atoms $i$ and $j$. The effect of varying $\rho_0$ can be seen in Fig. 1: Decreasing $\rho_0$ increases the range of the attractive part of the potential and softens the repulsive wall, thus widening the potential well. Values of $\rho_0$ appropriate to a wide range of materials have been catalogued (*10*). The intermolecular potential for $C_{60}$ molecules has a particularly short range relative to the equilibrium pair separation, with an effective value of $\rho_0 = 13.62$; rare gases are best described by medium-range potentials ($\rho_0 \sim 6$), whereas alkali metals have long-range interactions, for example, $\rho_0 = 3.15$ for sodium.

To understand the effect of the range of interatomic forces on the thermodynamics, it is helpful to partition the potential energy into three contributions:

$$V_M = -n_{nn} + E_{strain} + E_{nnn} \qquad (2)$$

The number of nearest neighbor contacts, $n_{nn}$, the strain energy, $E_{strain}$, and the contribution to the energy from non–nearest neighbors, $E_{nnn}$, are given by

$$\begin{aligned} n_{nn} &= \sum_{i<j,\, r_{ij}<r_0} 1 \\ E_{strain} &= \sum_{i<j,\, r_{ij}<r_0} [e^{\rho_0(1-r_{ij})} - 1]^2 \\ E_{nnn} &= \sum_{i<j,\, r_{ij}>r_0} e^{\rho_0(1-r_{ij})}[e^{-\rho_0(1-r_{ij})} - 2] \end{aligned} \qquad (3)$$

where $r_0$ is a nearest neighbor criterion. $E_{strain}$, which measures the energetic penalty for the deviation of a nearest neighbor distance from the equilibrium pair distance, is a key quantity in this analysis. This should not be confused with strain due to an applied external force. For a given geometry, $E_{strain}$ grows rapidly with increasing $\rho_0$ because the potential well narrows. This effect causes strained structures to be unfavorable for short-range potentials (*11*).

We used molecular dynamics and conjugate-gradient techniques to generate $\sim 10^3$ local minima for each potential energy surface at the intermediate value $\rho_0 = 6$. The simulations of bulk material were performed at constant volume in a cubic box containing 256 atoms at a reduced density of $\sqrt{2}$. We also studied clusters with 55 and 147 atoms; these sizes represent magic numbers for many systems, including the rare gases. The geometries of the local minima were subsequently reoptimized for ascending and descending integer values of $\rho_0$ (*12*). For the bulk material, the box size was scaled at each value of $\rho_0$ to keep the energy of the face-centered-cubic (fcc) minimum at a constant fraction of its zero-pressure energy. On changing $\rho_0$, a minimum may disappear from the potential energy surface. When this occurs, geometry optimization leads to a new minimum, and this causes the occasional discontinuities in the correlation diagrams (Fig. 2).

The lowest energy line in each correlation diagram at any given $\rho_0$ corresponds to the solid phase. For the bulk material (Fig. 2A), the lowest energy minimum is fcc for all values of $\rho_0$. The other low-energy minima are either close-packed structures misoriented with respect to the cubic box, or they are based on the fcc minimum and contain defects such as vacancy-interstitial pairs. The thick band of lines with positive

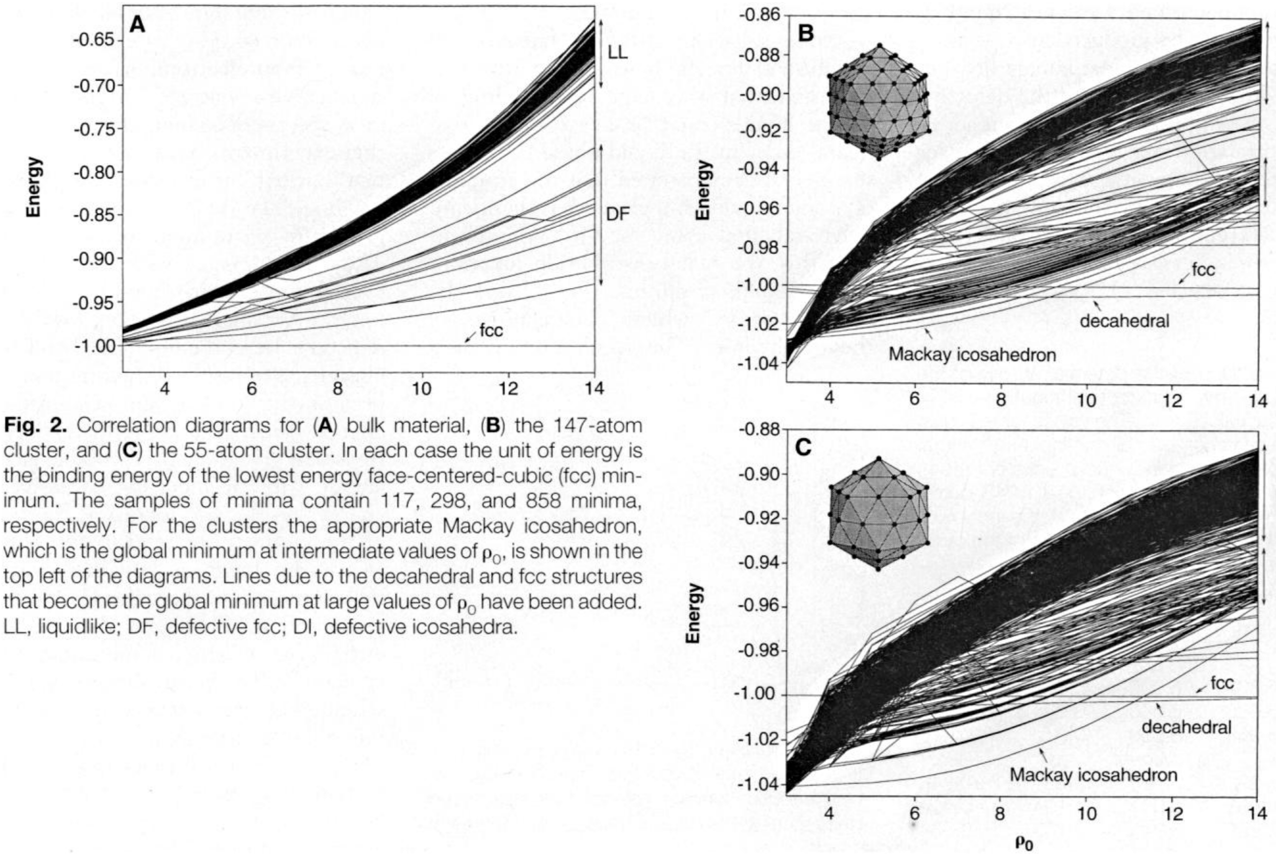

**Fig. 2.** Correlation diagrams for (**A**) bulk material, (**B**) the 147-atom cluster, and (**C**) the 55-atom cluster. In each case the unit of energy is the binding energy of the lowest energy face-centered-cubic (fcc) minimum. The samples of minima contain 117, 298, and 858 minima, respectively. For the clusters the appropriate Mackay icosahedron, which is the global minimum at intermediate values of $\rho_0$, is shown in the top left of the diagrams. Lines due to the decahedral and fcc structures that become the global minimum at large values of $\rho_0$ have been added. LL, liquidlike; DF, defective fcc; DI, defective icosahedra.

slope is due to minima found by quenching from the region of phase space corresponding to liquid behavior. We have sampled only a tiny fraction of all these "liquidlike" minima; for comparison, the number of minima corresponding to the liquidlike phase space of a 55-atom Lennard-Jones cluster has been estimated as $8.3 \times 10^{11}$ (*13*). It is because of this large configurational entropy and the greater vibrational entropy that the free energy of the liquid phase becomes lower than that of the solid phase as the temperature increases, leading to melting. For the bulk, the energy gap between these liquidlike minima and the fcc minimum clearly increases with $\rho_0$ (Fig. 2A). Thus, decreasing the range of the potential energetically destabilizes the liquid phase.

For the two clusters, Mackay icosahedra (*14*) (see Fig. 2, B and C) are the global minima at $\rho_0 = 6$. The series of low-energy lines in the correlation diagrams (Fig. 2, B and C) that run parallel to the lowest line result from Mackay icosahedra with surface defects. Rearrangements between these structures occur at energies just below that required for complete melting, leading to enhanced diffusion in the surface layer (*15*). In contrast to the bulk material, the structure of the solidlike phase of the cluster changes with $\rho_0$. At short range, decahedral and fcc structures become lower in energy than the Mackay icosahedron because the latter has a larger strain energy (*11*). The corresponding minima were not found in our original samples produced at $\rho_0 = 6$, so the lines due to the lowest energy decahedral and fcc minima (but not the defective structures based on them) have been added to the correlation diagrams. Hence, as for bulk material, the energy gap between the liquidlike minima and the lowest energy solid structure, be it icosahedral or decahedral, clearly increases as the range of interaction decreases (Fig. 2).

**Table 1.** Partition of the potential energy of the bulk phases into the different contributions of Eq. 2 at different values of $\rho_0$. The values for the liquid phase are averages over all the liquidlike minima. All energies are given in reduced units per atom. The nearest neighbor criterion, $r_0 = 1.243$, corresponds to the pair separation at the minimum between the first and second peaks of the radial distribution function.

| $\rho_0$ | $E$ | $n_{nn}$ | $E_{\mathrm{strain}}$ | $E_{nnn}$ |
|---|---|---|---|---|
| | | *Solid* | | |
| 6 | −6.822 | 6.000 | 0.000 | −0.822 |
| 10 | −6.050 | 6.000 | 0.034 | −0.097 |
| 14 | −5.958 | 6.000 | 0.042 | −0.016 |
| | | *Liquid* | | |
| 6 | −6.292 | 6.103 | 0.657 | −0.846 |
| 10 | −4.935 | 5.931 | 1.134 | −0.138 |
| 14 | −3.859 | 5.925 | 2.100 | −0.034 |

The energetic destabilization of the liquid phase seen for bulk material and clusters gives rise to a term in the free energy difference between the solid and liquid phases that increases rapidly with $\rho_0$. This term is likely to be the main range-dependent contribution to the free energy difference; the range dependence of the entropic contribution is likely to be less significant, because the entropy of both the solid and the liquid phases decreases as $\rho_0$ increases as a result of the narrowing of the potential wells and the attendant loss of accessible configuration space. Because the energetics of the gas phase are relatively unaffected by the range of the potential, for forces of sufficiently short range, the liquid phase is never thermodynamically stable. Thus, the destabilization of the liquid phase that has been noted in experiments and simulations of colloids and $C_{60}$ can be traced to the potential energy surface.

The physical basis for this behavior is simple. The structures of the liquidlike minima are inherently disordered, giving rise to a range of nearest neighbor distances: The first peak in the radial distribution function is broader than for the solid. The resulting strain energy rises rapidly as the range decreases and the potential wells narrow. This view was confirmed by examination of the three contributions to the energy for the two bulk phases at different values of $\rho_0$ (Table 1). The main contribution to the energy gap is found to be the larger strain energy of the liquid minima.

Our results can also be related to the structure of liquids. It was Frank who first suggested that the large supercooling of atomic liquids could be due to local icosahedral order in the liquid phase (*5*). It has since been demonstrated that the structure of atomic liquids and glasses has significant polytetrahedral character (*16*). Consistent with this, the radial distribution functions for the liquidlike minima (Fig. 3) lack the peak at $r = \sqrt{2}$, which is characteristic of the octahedron. The regular tetrahedron represents the densest local packing of spheres, but it cannot be used to pack all space. A polytetrahedral packing of space must therefore involve distorted tetrahedra, leading to local strain and a range of nearest neighbor distances. Polytetrahedral structure therefore underlies the larger strain energies in the liquid phase.

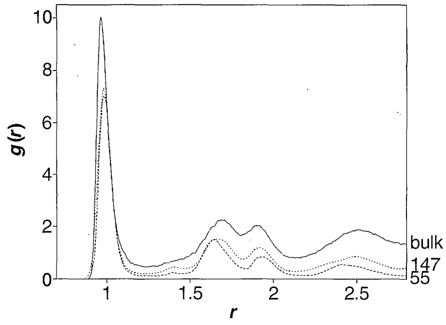

**Fig. 3.** Average radial distribution functions, $g(r)$, for the three sets of liquidlike minima at $\rho_0 = 6$. The distribution function has not been normalized with respect to the density because the volume of a cluster is not well defined.

Nelson has shown that polytetrahedral packings must involve defects called disclination lines (*17*). These lines connect atoms with coordination numbers different from the usual 12. If the disclination lines are arrayed periodically, one obtains crystalline structures called Frank-Kasper phases (*18*), which are closely related to many icosahedral quasi crystals (*19*). The known examples are generally alloys where some of the strain is relieved by the different atomic sizes. If the disclination lines are disordered, then one obtains structures typical of liquids and glasses. We can also understand the present results by considering the energetics of the disclination lines, which are most easily accommodated in systems bound by long-range forces. As the range of the potential decreases the energetic penalty for the local strains associated with the disclination lines increases, causing destabilization of the liquid phase.

One of the key differences between the correlation diagrams of the clusters and of bulk material is that for the two clusters the liquidlike minima actually become the lowest in energy at the small values of $\rho_0$, which are appropriate for alkali metals. This observation suggests an explanation for the change from electronic to geometric magic numbers at about 1500 atoms seen in the mass spectra of sodium clusters (*7*, *8*). Further experiments have shown that the clusters that exhibit electronic magic numbers are liquidlike, whereas those that exhibit geometric magic numbers are solidlike (*8*). These results agree with the behavior expected for clusters bound by long-range forces. At small sizes the lowest energy structures lie in the liquidlike band, and the cluster has a very low melting temperature because this band is almost continuous in energy. Hence, the cluster can adopt structures that give the most favorable electronic energy without incurring excessive strain energy. As the size increases, the behavior of the cluster must tend to the bulk limit where the band of liquidlike minima is higher in energy than the fcc solid for all values of $\rho_0$. Therefore, there must be a critical size at which a minimum based on an icosahedral, decahedral, or fcc packing scheme becomes lower in energy than the liquidlike minima. Above this size, the cluster will exhibit a geometric shell structure at temperatures below the melting point. For metals with shorter range potentials, geometric rather than electronic magic numbers are likely to dominate at relatively small sizes (*20*).

Our results also allow us to examine the development of the liquidlike state in clusters. The similarity of the radial distribution functions for the bulk and the cluster liquidlike minima (Fig. 3) shows that bulklike liquid structure develops at rather small cluster sizes. The only significant difference is the uniformly smaller value of the cluster radial distribution function, and this is simply due to the finite size. This similarity can easily be understood within the polytetrahedral model of liquid structure. Small clusters bound by medium-range forces have icosahedral growth sequences (*21*). For very small sizes (up to 31 atoms for the Lennard-Jones potential), the lowest energy sequence is purely polytetrahedral, although some close-packed character has developed by the time the 55-atom Mackay icosahedron is reached. Given the favorability of polytetrahedral structure for small clusters, it is not surprising that bulklike liquid character is seen at small sizes.

Similarly, the decreasing polytetrahedral character and increasing close-packed character of the Mackay icosahedron as the size increases can explain some of the differences in the correlation diagrams of the two clusters (Fig. 2, B and C). For the 55-atom cluster, the distinction between the top of the band of defective icosahedral structures and the band of liquidlike minima is unclear because of the relative structural similarity of the solid and the liquid at this small size. The energetic separation of these two bands of minima becomes larger as the size increases, giving the correlation diagrams the two-state character expected for a system that undergoes a first-order phase transition.

### REFERENCES AND NOTES

1. T. Coussaert and M. Baus, *Phys. Rev. E* **52**, 862 (1995).
2. M. H. J. Hagen and D. Frenkel, *J. Chem. Phys.* **101**, 4093 (1994).
3. A. P. Gast, C. K. Hall, W. B. Russel, *J. Colloid Interface Sci.* **96**, 251 (1983); E. J. Meijer and D. Frenkel, *J. Chem. Phys.* **100**, 6873 (1994); F. Leal Calderon, J. Bibette, J. Biais, *Europhys. Lett.* **23**, 653 (1993).
4. M. H. J. Hagen, E. J. Meijer, G. C. A. M. Mooij, D. Frenkel, H. N. W. Lekkerkerker, *Nature* **365**, 425 (1993); A. Cheng, M. L. Klein, C. Caccamo, *Phys. Rev. Lett.* **71**, 1200 (1993).
5. F. C. Frank, *Proc. R. Soc. London Ser. A* **215**, 43 (1952).
6. M. R. Hoare, *Ann. N.Y. Acad. Sci.* **279**, 186 (1976).
7. T. P. Martin, T. Bergmann, H. Göhlich, T. Lange, *Chem. Phys. Lett.* **172**, 209 (1990).
8. T. P. Martin, U. Näher, H. Schaber, U. Zimmermann, *J. Chem. Phys.* **100**, 2322 (1994).
9. F. H. Stillinger and T. A. Weber, *Science* **225**, 983 (1984).
10. D. J. Wales, L. J. Munro, J. P. K. Doye, *J. Chem. Soc. Dalton Trans.*, in press.
11. J. P. K. Doye, D. J. Wales, R. S. Berry, *J. Chem. Phys.* **103**, 4234 (1995).
12. Further simulations and geometry optimizations indicate that this method gives a good representation of the potential energy surface away from $\rho_0 = 6$ for bulk material and liquid clusters. For the solid clusters, though, there is a well-understood change in structure (*11*) that affects the low-energy region of the potential energy surface.
13. J. P. K. Doye and D. J. Wales, *J. Chem. Phys.* **102**, 9659 (1995).
14. A. L. Mackay, *Acta Crystallogr.* **15**, 916 (1962).
15. R. E. Kunz and R. S. Berry, *Phys. Rev. Lett.* **71**, 3987 (1993).
16. D. R. Nelson and F. Spaepen, *Solid State Phys.* **42**, 1 (1989).
17. D. R. Nelson, *Phys. Rev. Lett.* **50**, 982 (1983); *Phys. Rev. B* **28**, 5515 (1983).
18. F. C. Frank and J. S. Kasper, *Acta Crystallogr.* **11**, 184 (1958); *ibid.* **12**, 483 (1959).
19. C. L. Henley and V. Elser, *Philos. Mag. B* **53**, L59 (1986).
20. D. Rayane *et al.*, *Phys. Rev. A* **39**, 6056 (1989).
21. J. A. Northby, *J. Chem. Phys.* **87**, 6166 (1987).

22. We thank the Royal Society (D.J.W.) and the Engineering and Physical Sciences Research Council, and Gonville and Caius College (J.P.K.D.) for financial support.

25 August 1995; accepted 8 November 1995

---

# Reversible Encapsulation of Disc-Shaped Guests by a Synthetic, Self-Assembled Host

Robert M. Grotzfeld, Neil Branda, Julius Rebek Jr.*

Here, the synthesis of a bowl-shaped molecule is described and evidence of its reversible dimerization by means of hydrogen bonds is presented. The dimer features a flattened spherical cavity of peculiar symmetry and acts as a host for the encapsulation of guest molecules of complementary shape. Encapsulation of aromatic guests in chloroform solution and of cyclohexane in *p*-xylene solution was demonstrated by nuclear magnetic resonance experiments. The passage of guests into and out of the cavity is slow and occurs on a time scale of hours. The system was used to explore the effects of size, shape, and solvation on molecular recognition coupled with assembly.

Previous efforts in the synthesis of self-assembled molecular capsules have led to small cavities capable of sequestering methane (*1*) and large cavities that can accommodate molecules of the size of adamantanes (*2*). These earlier capsules present roughly spherical interiors, and their recognition properties reflect preferences for guests of this shape. Here, we introduce an assembly of intermediate size and unusual ($D_{3d}$) symmetry. The overall shape resembles that of a jelly doughnut, and it features a flattened spherical interior cavity. This assembly encapsulates disc-like molecules—for example, benzene or cyclohexane.

As in earlier designs, the assembly involves the reversible dimerization of self-complementary monomers. These associate by interlocking the concave and convex parts of the two monomers and are held together by weak intermolecular forces. The new architectural features are presented schematically in Fig. 1, wherein the threefold symmetry of the monomers is emphasized and the curvature of the dimeric assembly is exaggerated.

The driving force for assembly takes advantage of modest directional characteristics of hydrogen bonds. These are common to many other studies of self-assembly (*3*), and we have found that glycoluril units (for example, **4** in Fig. 2) provide a particularly rich source of donor and acceptor functions desirable for self-complementary structures (*1*). Any number of rigid aromatic nuclei can act as spacers between the glycoluril units; the spacer determines the dimensions and shape of the molecular assembly (*4*). A triphenylene derivative (**2**) was chosen as the spacer, so that the ceiling and floor of the assembled capsule consisted of aromatic π surfaces. The fusion of three glycoluril units to the spacer with an all-cis stereochemistry (as in **5**) imparts a curvature to the structure and forces the association to occur in only one way; the maximum number of hydrogen bonds (12) can be achieved only when two molecules present their concave faces to each other.

The synthesis began with the reaction of bromofluoroxylene **1** with magnesium to give hexamethyltriphenylene **2**, in what is formally a benzyne trimerization. Bromination of **2** gave hexakis(bromomethyl)triphenylene **3**, which was used without purification in the alkylation of glycoluril **4**.

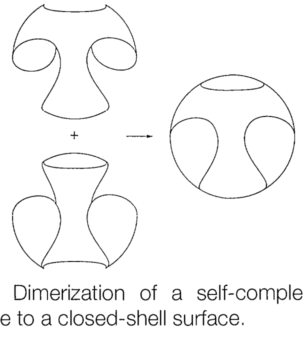

**Fig. 1.** Dimerization of a self-complementary structure to a closed-shell surface.

---

Department of Chemistry, Massachusetts Institute of Technology, 77 Massachusetts Avenue, Cambridge, MA 02139, USA.

*To whom correspondence should be addressed.